



THE UNIVERSITY *of* EDINBURGH

## Edinburgh Research Explorer

### FRP Strains in FRP Wrapped Columns

**Citation for published version:**

Chen, JF, Ai, J & Stratford, TJ 2007, FRP Strains in FRP Wrapped Columns. in *Advanced Composites in Construction 2007: ACIC 2007: Proceedings of the Third International Conference, Held at the University of Bath, UK on 2nd - 4th April 2007*. pp. 147-155, ACIC 07 - Advanced Composites in Construction Conference 2007, Bath, United Kingdom, 2/04/07. <<http://www.netcomposites.com/calendar/acic-07---advanced-composites-in-construction-conference-2007/601>>

**Link:**

[Link to publication record in Edinburgh Research Explorer](#)

**Document Version:**

Publisher's PDF, also known as Version of record

**Published In:**

Advanced Composites in Construction 2007

**General rights**

Copyright for the publications made accessible via the Edinburgh Research Explorer is retained by the author(s) and / or other copyright owners and it is a condition of accessing these publications that users recognise and abide by the legal requirements associated with these rights.

**Take down policy**

The University of Edinburgh has made every reasonable effort to ensure that Edinburgh Research Explorer content complies with UK legislation. If you believe that the public display of this file breaches copyright please contact [openaccess@ed.ac.uk](mailto:openaccess@ed.ac.uk) providing details, and we will remove access to the work immediately and investigate your claim.



# FRP STRAINS IN FRP WRAPPED COLUMNS

J. F. Chen<sup>1</sup>, J. Ai<sup>2</sup>, T. J. Stratford<sup>3</sup>

<sup>1,2,3</sup> *Institute for Infrastructure and Environment, The University of Edinburgh*

**Abstract:** Extensive research has been undertaken on strengthening concrete columns using FRP wraps. Recent research has extended this technique into strengthening steel tubular and concrete filled steel tubular columns. The behaviour of FRP confined concrete columns is now well understood and accurate models for both design and analysis are available. The only gap in knowledge is perhaps the lack of understanding of why the FRP failure strain in FRP wrapped columns is significantly lower than the ultimate tensile strain in a coupon test and its quantification. This paper presents a preliminary study tackling this problem.

**Keywords:** *Concrete columns, steel tubular columns, strengthening, FRP, strain*

## 1 Introduction

There has been extensive research into the use of FRP wrapping to strengthen concrete and concrete-filled steel columns [e.g.: 1-5]. This technique is often favoured for the simplicity with which it can be applied and consequent economic benefits compared to traditional methods of strengthening, and there are numerous applications around the world [6,7].

To design FRP strengthening for a column the designer requires a model for the concrete confined within the wrap and the stress/strain that results in the FRP. Various models for concrete confined by FRP have been developed, so that accurate methods are now available for design [3,4,6,8]. The strain in the FRP is compared to an allowable value to check that failure does not occur. Numerous experiments have shown that the wrap fails at a hoop strain significantly lower than the FRP ultimate rupture strain determined from coupon tensile tests [1,3,4,9]. There can be a variety of possible causes for this phenomenon. Lam and Teng [10] conducted the first carefully planned comparative experiments attempting to clarify the causes for reduced strain capacity of FRP when used to confine concrete. They concluded that there are at least three factors: (1) the curvature of FRP jacket which results in a reduced strain capacity; (2) the deformation non-uniformity of cracked concrete which leads to non uniform strain distribution in the FRP; and (3) the existence of an overlapping zone in which the measured strains are much lower than strains elsewhere. The effect of adhesive bonding on the hoop rupture strain in a GFRP

jacket was also investigated by Harries and Carey [11] but this effect was not clearly established by the test results.

Other causes for the reduced strain capacity of FRP when used to confine concrete may include geometric imperfections of the column, non-uniform bonding between the FRP and the concrete, the biaxial stress state in the FRP composite, misalignment of fibres, and geometrical discontinuity at the overlapping zone of the FRP. Although the effect of fibre orientation has been the subject of several studies [e.g. 5], the effect of other factors has not been investigated to the best knowledge of the authors.

The aim of this paper is to establish a rational finite element model to examine the effect of the geometrical discontinuity at the two ends of the FRP sheet on the FRP strain at failure in FRP-wrapped concrete or concrete filled steel columns. It is believed that the geometrical discontinuities at these two ends of the overlap zone can cause significant local bending strains in the FRP, leading to a greatly reduced average failure strain of the FRP. Four different models of FRP wrapped columns are analysed using the finite element method.

## 2 Geometry of an FRP wrapped column

This study considers a circular column wrapped with a single layer of sheet FRP (Fig. 1a). The geometry of the column can be described using a polar coordinate system (Fig. 1b). The FRP starts at an angle  $\theta=0^\circ$  on the inside of the wrap and finishes at  $\theta=465^\circ$  on the outside,

<sup>1</sup> Lecturer, J.F.Chen@ed.ac.uk

<sup>2</sup> PhD student, J.Ai@ed.ac.uk

<sup>3</sup> Lecturer, T.J.Stratford@ed.ac.uk

resulting in an overlap zone of  $\alpha=105^\circ$ . The change in radius necessary for the outer layer of FRP to overlap the inner layer is described by a transition zone of length  $\beta=30^\circ$ . A sinusoidal transition is assumed, so that the inner and outer surfaces of the FRP within the transition zone are expressed as:

$$r_i = R + t_a + \frac{t_a + t_f}{2} \left( 1 - \cos \left\{ \frac{\pi}{\beta} (\theta - (2\pi - \beta)) \right\} \right) \quad (1a)$$

$$r_o = r_i + t_f \quad (1b)$$

where,  $r_i$  and  $r_o$  are the radius of the inner and outer surfaces of the FRP within the transition zone respectively,  $R$  is the radius of the un-strengthened column,  $t_f$  is the thickness of the FRP sheet, and  $t_a$  is the thickness of the adhesive layer outside of the transition zone. The values adopted for this study for these parameters are listed in Table 1.

The system contains three interfaces (Fig. 1b): the interface between the column and adhesive, that between the inner surface of the FRP and the adhesive, and that between the outer surface of the FRP and the adhesive. For such a system under radial expansion, it is expected that there are stress concentrations:

- on the outer surface of the FRP at  $\theta=105^\circ$ , adjacent to the end of the outer FRP layer (location A).
- on the inner surface of the FRP at  $\theta=360^\circ$ , adjacent to the end of the inner FRP layer (location B).

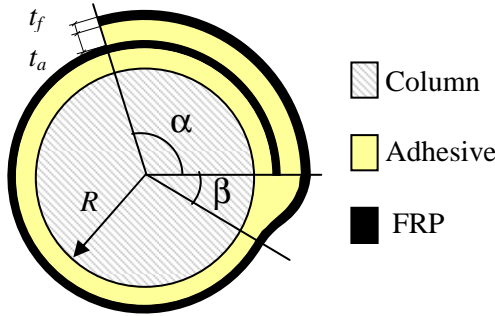


Figure 1a: An FRP wrapped column: schematic view

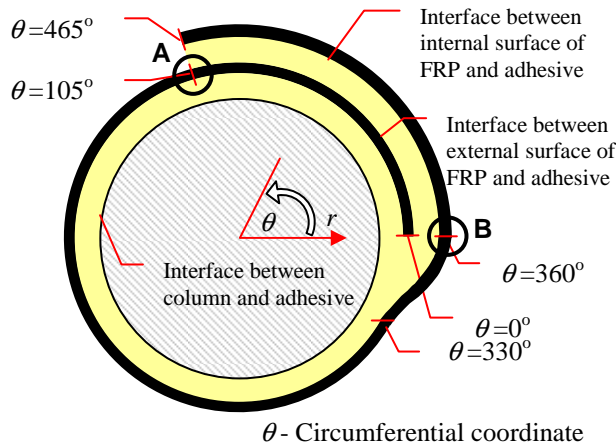


Figure 1b: Coordinate system and interfaces

### 3 Properties of the FRP composite

FRP composites are orthotropic materials. Their mechanical properties are affected by the fibre architecture (orientation and distribution) and the relative proportions of the two phases (fibre and matrix). The macro properties of the composite may be estimated from the fibre architecture and fibre volume fraction using the “law of mixtures” (LoM) [12].

The current study assumes the fibre and adhesive properties given in Table 2. These values are typical for wet lay-up strengthening using carbon fibres and an epoxy bonding resin. It is assumed that both the matrix of the composite and the bonding adhesive have the same properties. Assuming a unidirectional fibre architecture (in hoop direction) and 60% fibre volume ratio are used, the deduced macro properties of the FRP composite based on the LoM are given in Table 3.

Table 1: Geometry of the modelled column

Radius of column ( $R$ )	(mm)	82.5
Thickness of FRP ( $t_f$ )	(mm)	0.1
Thickness of adhesive ( $t_a$ )	(mm)	1.0
Angle of overlap ( $\alpha$ )	(deg.)	105
Angle of transition ( $\beta$ )	(deg.)	30

Table 2: Properties of fibre, matrix and adhesive

	Young's Modulus (GPa)	Poisson's ratio [13]
Fibre	230	0.20
Matrix and adhesive	3.0	0.35

Table 3: Derived properties of the FRP composite

$E_{11}$ (GPa)	139	$G_{23}$ (GPa)	3.70
$E_{22}$ (GPa)	15.5	$\nu_{12}$	0.26
$E_{33}$ (GPa)	15.5	$\nu_{13}$	0.26
$G_{12}$ (GPa)	4.26	$\nu_{23}$	0.26
$G_{13}$ (GPa)	4.26		

Note: (a) Direction 1 is the fibre direction, directions 2 and 3 are perpendicular to the fibre direction; (b) Other Poisson's ratios can be derived from  $E_{ij}/E_{ji} = \nu_{ij}/\nu_{ji}$ , where  $i, j = 1, 2, 3$ .

### 4 Loading schemes and boundary conditions

Only the FRP and the bonding adhesive are modelled in the finite element analysis; the concrete is not included. The action of the confined concrete on the FRP wrap may be obtained from a variety of models [1,3,4,6]. This paper examines four different loading schemes that describe the action of the confined concrete on the strengthening materials (Table 4). Either prescribed displacements or internal pressure loading are applied at the adhesive-concrete interface.

A 1mm prescribed radial displacement is applied in the first two loading schemes (LB1 and LB2). For load case LB1, the circumferential displacement is fixed (as might be expected at the adhesive-concrete interface).

LB1 simulates the case when the column is under uniform expansion and there is no debonding between the FRP and the column. However, for load case LB2, circumferential displacements are unrestrained. This would be close to an extreme situation where the column is under uniform expansion but the FRP has debonded from the column around the whole circumference (but the FRP overlap has not failed) with negligible frictions.

An internal pressure load is applied in loading schemes LB3 and LB4. Again, the circumferential displacement is either unrestrained (LB3) or fixed (LB4). The former represents the situation where the confined column induces a uniform pressure on the FRP and the bond between the FRP and the column is intact. The later is close to another extreme case where the FRP is completely debonded from the column but the overlap zone remains intact, forming an integral ring. The applied internal pressure of 2.48MN/m gives 1mm radial displacement at the inside of the adhesive for an equivalent single layer strengthening system that does not contain an overlap.

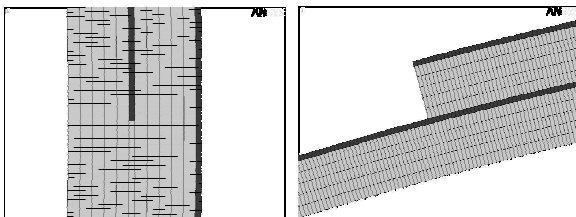
**Table 4:** Loading schemes and boundary conditions

Loading schemes	Short title	Force (MN/m)	Displacement (mm)	
			Radial DOF	Circumferential DOF
Displacement	LB1		1	Fixed
	LB2		1	Free
Internal pressure	LB3	2.48	Free	Free
	LB4	2.48	Free	Fixed

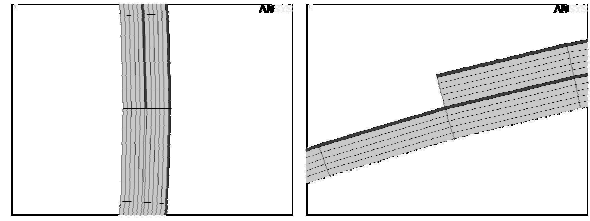
## 5 Finite Element Modelling

### 5.1 Mesh and mesh convergence

The system was modelled using the general finite element analysis package ANSYS. A uniform mesh containing equally sized 4-node quadrilateral elements was used. Fig. 2 shows details of the mesh at the two ends of the overlap. A mesh convergence study was conducted using loading scheme LB1. The circumferential element size varied from a minimum of 0.05° to a maximum of 3.0°. The FRP was represented by one layer of elements and the adhesive represented by five layers of elements in all the models. Figs. 2a and 2b show parts of the finest and coarsest meshes, respectively.

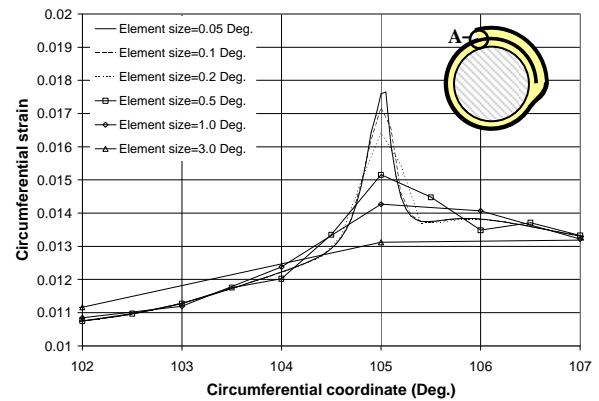


(a) Near  $\theta=0^\circ$  and  $360^\circ$  (b) near  $\theta=105^\circ$  and  $465^\circ$   
**Figure 2a:** FE mesh details: element size=0.05°

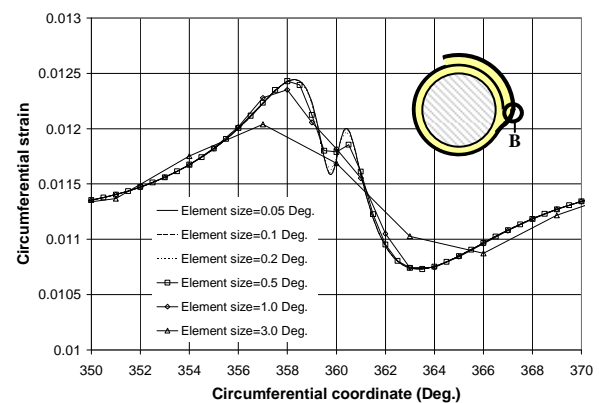


(a) Near  $\theta=0^\circ$  and  $360^\circ$  (b) near  $\theta=105^\circ$  and  $465^\circ$   
**Figure 2b:** FE mesh details: element size=3.0°

Fig. 3 shows how the circumferential strain at the outside of the FRP varied during the mesh convergence study. The strain distributions are shown at two significant positions: (a) at the end of the outer piece of FRP (Fig. 3a) and (b) adjacent to the end of the inner piece of FRP (Fig. 3b). Clearly a substantial stress concentration exists at both locations and a coarse mesh significantly reduces the peak stresses, especially at the external surface of the inner layer of FRP near location A.



(a) On the inner layer of FRP near location A



(b) On the outer layer of FRP near location B

**Figure 3:** Effect of mesh size on circumferential FRP strain distribution along the external surface under LB1

Fig. 4 shows how the maximum strain in the FRP (from Fig. 3a) varies with the element size. An element size of 0.1° (about 0.14 mm in circumferential direction) was deemed sufficiently accurate for this initial

investigation and this mesh was used in all calculations in the rest of the paper.

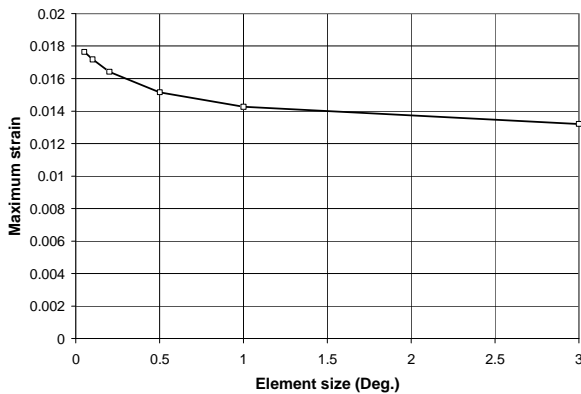


**Figure 4:** Effect of mesh size on the maximum circumferential strain in the FRP under LB1

## 5.2 Effect of loading and boundary conditions

The four different loading schemes and boundary conditions were examined to determine the most appropriate model for the action of the confined concrete on the strengthening system.

### 5.2.1 Displacement loading

Fig. 5 plots the distribution of circumferential strain within the outer surface of the FRP for load cases LB1 and LB2 (a prescribed 1mm radial displacement). The strain is plotted against the circumferential position, from the inner end to the outer end of the FRP (as defined in Fig. 1b). Significant changes in the strain occur at each of the geometric discontinuities: the inner end of the FRP ( $0^\circ$ ), the outer end of the FRP ( $105^\circ/465^\circ$ ), and the transition zone ( $330^\circ$  to  $360^\circ$ ).

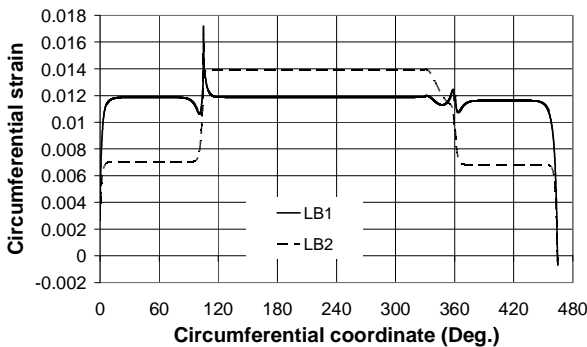


**Figure 5:** Circumferential strain along the outer surface of the FRP under displacement loading.

The circumferential displacement is fixed for LB1 and consequently the circumferential strain in the FRP is the same within the overlap zone as outside the overlap zone ( $\sim 0.012$ ). In LB2, however, the circumferential displacement is unrestrained, and the strain within the overlap zone is half the strain elsewhere in the FRP. This is a necessary condition to satisfy equilibrium because of the doubling in stiffness

that results from two layers of FRP within the overlap zone.

Although the strains outside of the overlap zone are larger under LB2 than those under LB1 under the same prescribed radial displacement, the stress concentration near location A under LB1 is more significant than under LB2.

Fig. 6 shows the circumferential strain in the adhesive along the interface between the column and adhesive. Under LB1, the strain is uniform as no circumferential displacement is permitted. The free circumferential moment under LB2 results in strains outside of the overlap zone that are twice as big as those inside the joint; as required to satisfy equilibrium. Significant variations are experienced at the transitions between these two zones. Away from this interface, very significant strain variations also exist in the adhesive, especially near the two ends of the FRP.

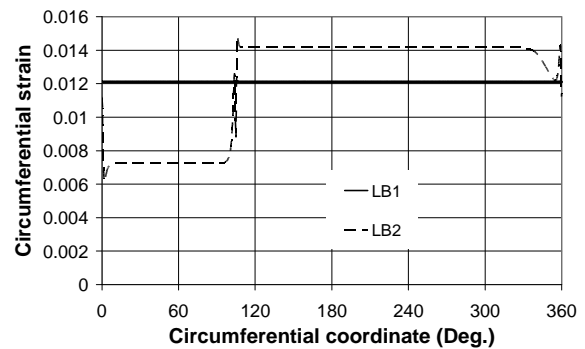


**Figure 6:** Circumferential strain in the adhesive along the interface between column and adhesive under displacement loading

### 5.2.2 Internal pressure loading

Figs 7 and 8 plot the circumferential strain in the FRP and adhesive for the internal pressure loading cases, LB3 and LB4. In these cases, the radial displacement is not prescribed. The strains within the overlap zone are much lower than those outside in both cases.

If the circumferential displacement is restrained (LB4), the strain distribution is fairly uniform both within and outside the overlap zone, except for near its two ends. The FRP strain within the overlap zone is half of that outside, to satisfy equilibrium requirement (Fig. 7). Within the overlap zone, the circumferential strain in the adhesive adjacent to the column is also half the value found outside the overlap (Fig. 8).

The circumferential displacement is not restrained in load case LB3, resulting in very large bending strains in the FRP (Fig. 7). Similar bending strain is also seen in the adhesive at the interface between the column and the adhesive (Fig. 8). Clearly, the resulting deformed shape of the FRP strengthening is not compatible with the confined concrete in this case (Fig. 9).

The four loading cases represent four extremes, but LB3 (under uniform internal pressure with circumferential direction unrestrained) is unlikely to occur because its deformed shape is not compatible with the circular form of the column. Therefore, in reality the

strain distributions are likely to lie somewhere between LB1, LB2 and LB4. Among these three load cases, LB1 (in which the radial and circumferential displacements are prescribed) results in the greatest peak strains, and hence is conservative. LB1 is used throughout the remainder of the paper.

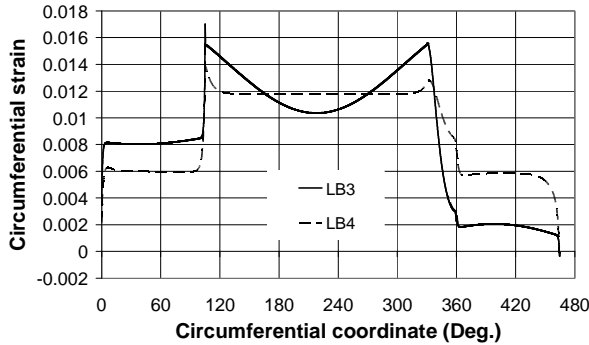


**Figure 7:** Circumferential strain along external surface of FRP under internal pressure loading.

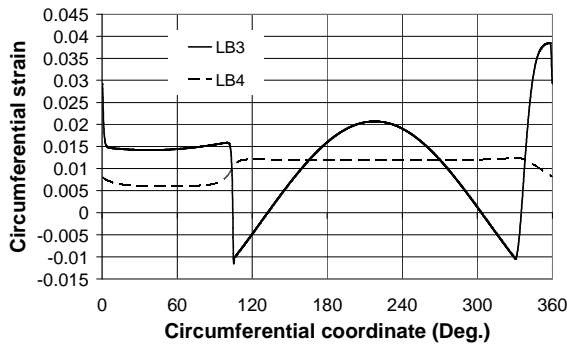


**Figure 8:** Circumferential strain in adhesive along the interface between column and adhesive under internal pressure loading.

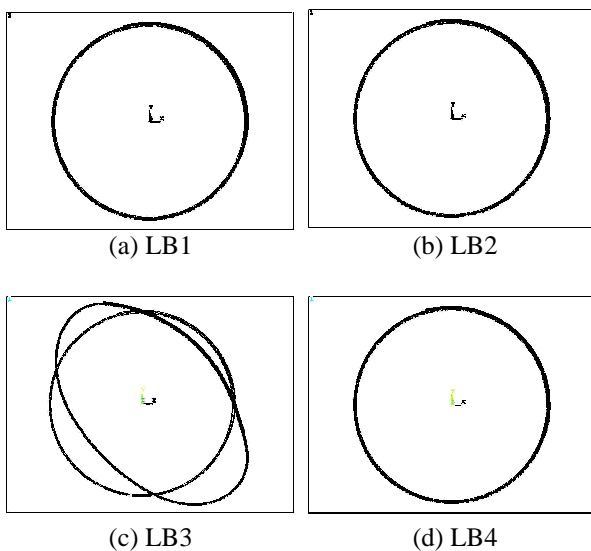


**Figure 9:** Deformation of FRP.

### 5.3 Effect of FRP orthotropy

The significance of the FRP's orthotropic material properties was assessed by comparing the

circumferential strain distribution in the FRP using isotropic and orthotropic material models, shown in Fig. 10. Fig. 10a plots the strain at the inside and outside surfaces of the FRP predicted by each material model. Figs. 10b and 10c give the detailed strain distribution adjacent to each end of the overlap zone (at 105° and 360°).

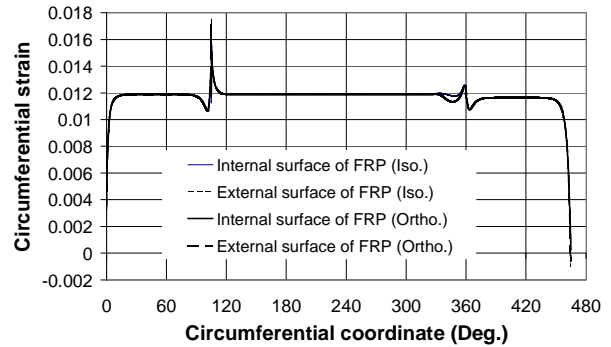


**Figure 10a:** Circumferential strain in the outer and inner FRP surfaces using different material models

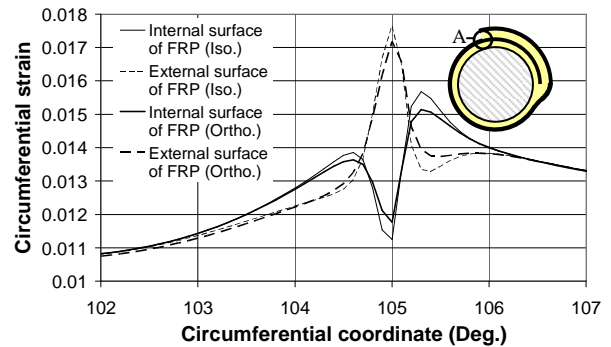


**Figure 10b:** Circumferential strain in FRP surfaces using different material models (near location A)

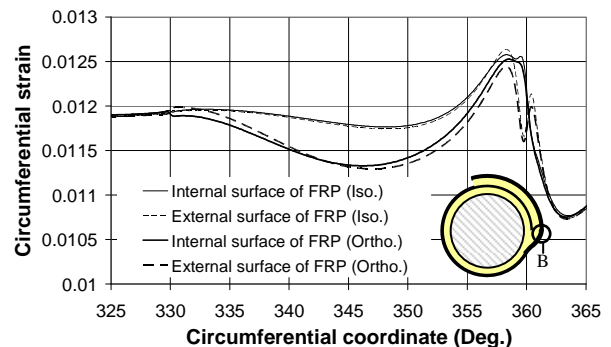


**Figure 10c:** Circumferential strain in FRP surfaces using different material models (near location B)

It can be seen that the difference between results from the isotropic and orthotropic models is small: the maximum circumferential strain is reduced by around 3% by using orthotropic material properties. The magnitude of the radial strain in the FRP (Fig. 11) is also slightly lower when an orthotropic material is used. Whilst it would be conservative to use an isotropic material for analysis, an orthotropic representation is

obviously more rigorous for FRP composites, and all the results presented in this paper have been predicted using an orthotropic material representing the FRP composites (unless stated otherwise).

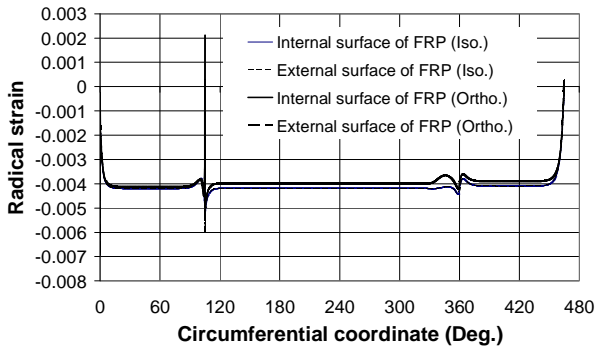


**Figure 11:** Radial strain on FRP surfaces using different material models

## 6 Numerical results

### 6.1 Strains within the FRP

The circumferential strains predicted by the analysis are shown in Fig. 12. The strains are plotted at the extreme fibres of the FRP. Any difference between the strain at the inside and outside edges resulted from curvature (and hence bending) of the FRP.

Fig. 12a shows the strain variation along the FRP strengthening sheet, from its inner ( $0^\circ$ ) to its outer end ( $465^\circ$ ). The strain is very small at the inner end but it increases rapidly as the angle increases and reaches a plateau at about  $30^\circ$ . It is fairly uniform after that, except around the two locations adjacent to the two ends of the FRP. The strain reduces rapidly within about  $15^\circ$  from the outer end.

There are significant fluctuations in strain in the region of locations A and B in the strengthening FRP, adjacent to the two ends of the FRP. These are due to the local geometric discontinuities (Fig. 1b). Figs. 12b and 12c focus on the strain distributions around locations A and B. The circumferential strain distribution across the FRP can also be seen in the contour plots in Fig. 13.

The outer end of the FRP tends to peel away from the cylinder and thus pulls the inner layer of FRP outwards, resulting in significant outward bending strains at location A ( $\theta=105^\circ$ ). The bending strains are reversed a short distance to either side of location A, but they are much less significant than at A. The peak tensile strain in the outer surface of the FRP at location A is 0.017, which is about 40% higher than the strain away from the local discontinuities (or calculated based upon a simple hoop model as used in design), 0.012. Alternatively, the average strain (0.012) is only about 70% of the peak tensile strain (0.017). About 20% of this peak stress is due to bending.

FRP composites are almost linear-elastic up to failure with uni-directional fibres; hence fracture will occur when the peak tensile strain reaches the ultimate tensile strain of the material. Where high local tensile

strains exist, the strain elsewhere in the FRP is consequently lower than the failure strain. In this particular example, the finite element prediction is about 70% of the FRP ultimate tensile strain, which is well within the range of experimental observations [4].

It should be noted that the predicted local stress concentration is within a very small zone.  $0.1^\circ$  from the outer end of the FRP (location A), the tensile strain is much lower than the peak strain. ( $1^\circ$  represents about 1.4mm length in the present example). The rapid variation of strain within such a small zone means that detecting the peak strain using normal measurement techniques such as electrical resistance strain gauges is not possible, which may explain why the stress concentration within this zone has not been observed experimentally. It shall also be emphasised that the actual strain concentration is likely to be sensitive to the geometry of the adhesive at the end of the FRP as well as the plastic properties of the adhesive. The present prediction, using a linear elastic material model for the adhesive which is flush with the end of the FRP, probably represents the worst scenario.

The inner end of the strengthening FRP tends to pull the outer layer of FRP inwards, resulting in inwards bending at location B ( $\theta=360^\circ$ ). As this end is confined by the outer layer of FRP, the bending strains here are relatively small compared to those at location A. The peak strain is also smaller, about 5% over the value remote from the end of the FRP. Fig. 13b shows that the strain gradient is much smaller here than that at location A (Fig. 13a).

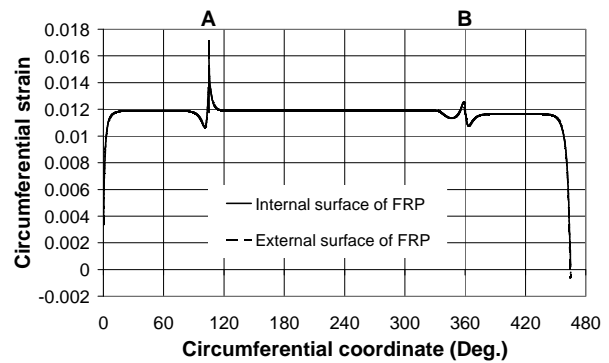


**Figure 12a:** Circumferential strain on FRP surfaces

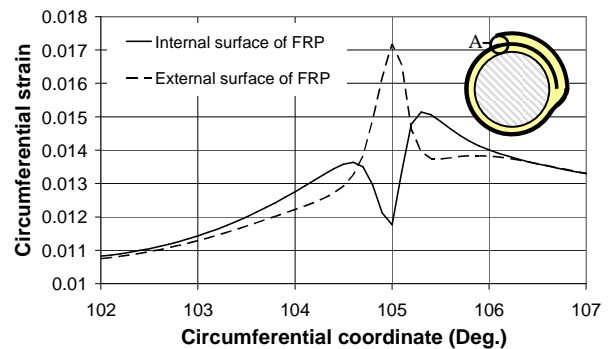


**Figure 12b:** Circumferential strain on FRP surfaces near location A

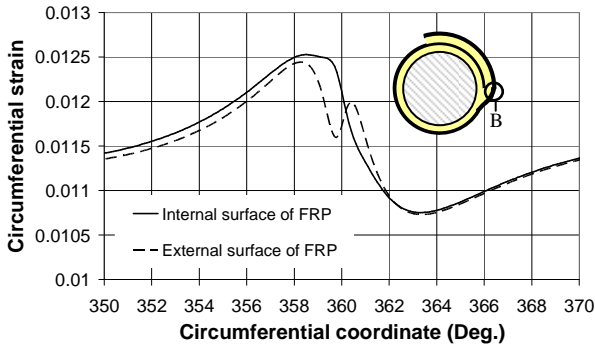


**Figure 12c:** Circumferential strain on FRP surfaces near location A

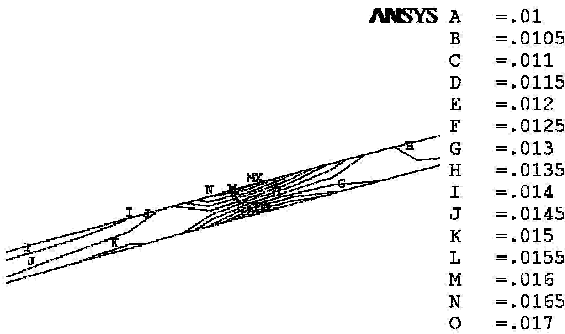


**Figure 13a:** Circumferential strain distribution in FRP near location A

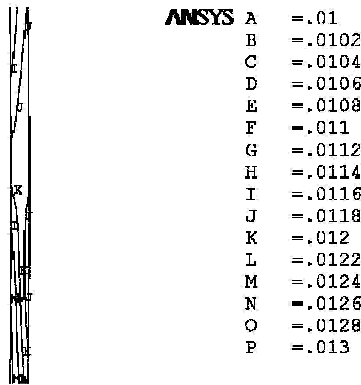


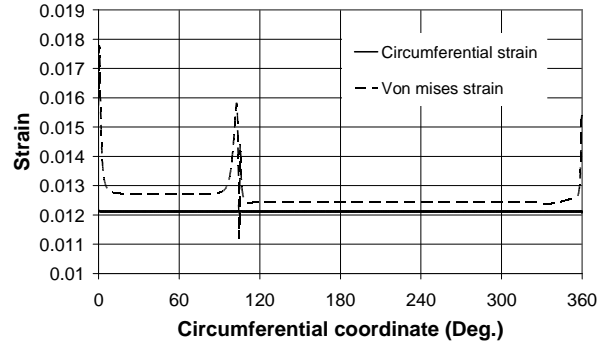
**Figure 13b:** Circumferential strain distribution in FRP near location B

## 6.2 Strains within the bonding adhesive

The adhesive bonds the strengthening FRP to the concrete column, and also bonds the two layers of FRP together within the overlap zone. The circumferential strains in the adhesive have been examined using the finite element model; however, radial strains also exist within the adhesive. In particular, the peeling strains near the outer end of the FRP could cause the FRP to separate from the concrete. The von Mises strain has been used to assess because it reflects the combined effect of all the strain components.

Fig. 14 plots both the circumferential and von Mises strains within the adhesive immediately adjacent to the concrete column. Although the circumferential strain is uniform around the whole column under the

given loading case, the von Mises strains are usually larger due to the existence of radial strains in the adhesive. There are very significant variations in von Mises strain adjacent to each end of the FRP, due to tensile radial stresses, with a peak strain of 0.018 at  $\theta > 0^\circ$ .



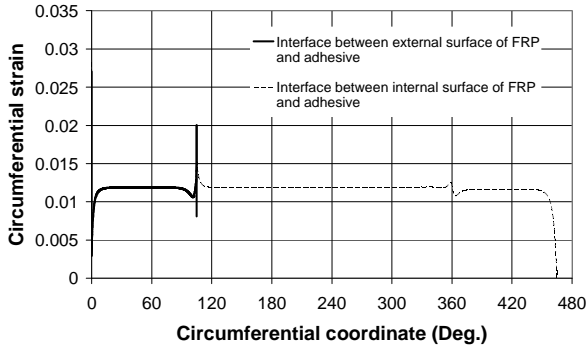
**Figure 14:** Circumferential and von Mises strains in the adhesive along the interface between column and adhesive

Fig. 15 shows the adhesive strains immediately adjacent to the FRP. The strain along the internal surface of the FRP is plotted from the inner end ( $0^\circ$ ) to the outer end ( $465^\circ$ ) of the strengthening FRP. Adhesive strains along the outside surface of the FRP are only present along the overlapping zone ( $0^\circ$  to  $105^\circ$ ) because the outer surface is free for  $\theta > 105^\circ$ .

Fig. 15a shows that there are peaks in the circumferential adhesive strain at  $\theta = 0^\circ$ ,  $105^\circ$  and  $360^\circ$ , with the largest peak at  $\theta = 0^\circ$  and smallest peak at  $\theta = 360^\circ$ . However, large strains around the inner end of the FRP (at  $\theta = 0^\circ$  and  $360^\circ$ ) are not really a problem because of the confinement provided by the outer layer of the FRP, so it does not matter even if micro cracks occur there. In contrast, large stresses near the outer end of the FRP (at  $\theta = 105^\circ$ ) can lead to separation of the FRP. The detailed strain distribution near  $\theta = 105^\circ$  is shown in Fig. 15b, where a large peak tensile strain of 0.02 is seen at the interface between the adhesive and the outer surface of the FRP.

Figs. 15c and 15d plot the von Mises strains. The effect of the radial strain adjacent to the inner layer of FRP is significant: the peak at  $\theta = 105^\circ$  is substantially increased with a value of 0.035 in the adhesive adjacent to the outer layer of FRP, which is similar to that at  $\theta = 0^\circ$ . Another visible effect from the radial strain is another peak at  $465^\circ$  (the outer end of the FRP) where the circumferential strain is zero (Fig. 15a). These strains results from peeling of the outer end of the FRP away from the column, and will govern the performance of the bonding system. Further details can be seen in contour plots of circumferential and von Mises strain adjacent to the two ends of the FRP (Fig. 16).





**Figure 15a:** Circumferential strain in adhesive along the interfaces between the FRP and adhesive

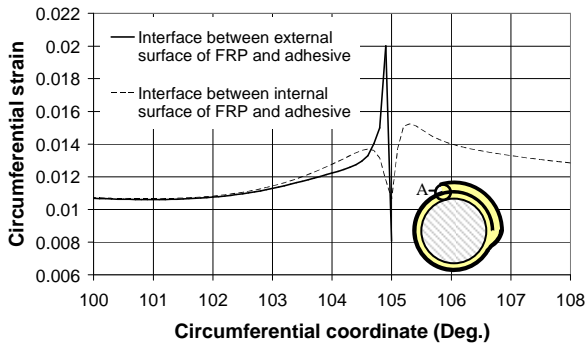


**Figure 15b:** Circumferential strain in adhesive along the interfaces between FRP and adhesive (near A)

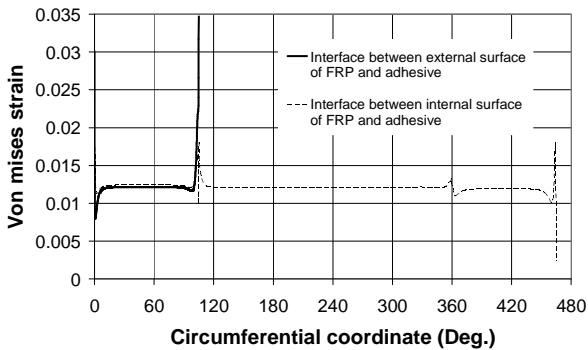


**Figure 15c:** von Mises strain in adhesive along the interfaces between FRP and adhesive

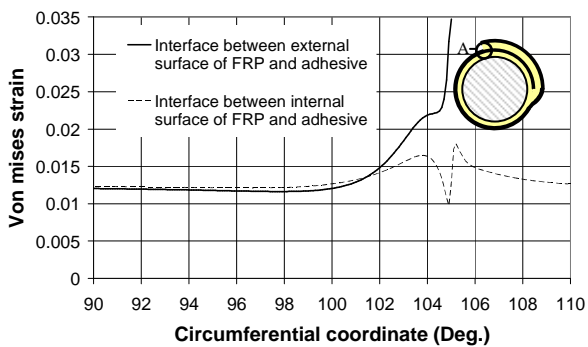


**Figure 15d:** von Mises strain in adhesive along the interfaces between FRP and adhesive (near location A)

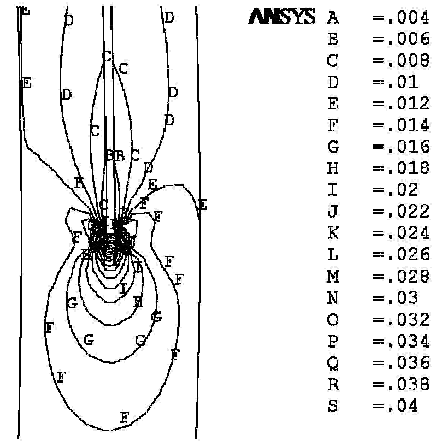


**Figure 16a:** Circumferential strain in the adhesive near the inner end of the FRP (B)

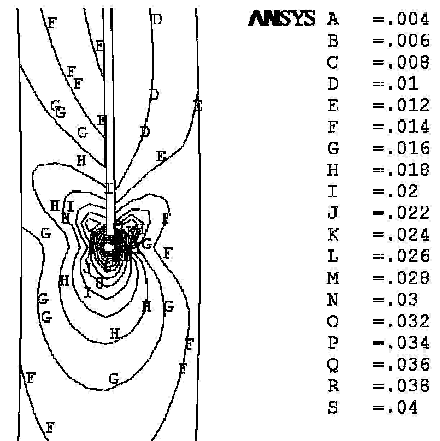


**Figure 16b:** von Mises strain in the adhesive near the inner end of the FRP (B)

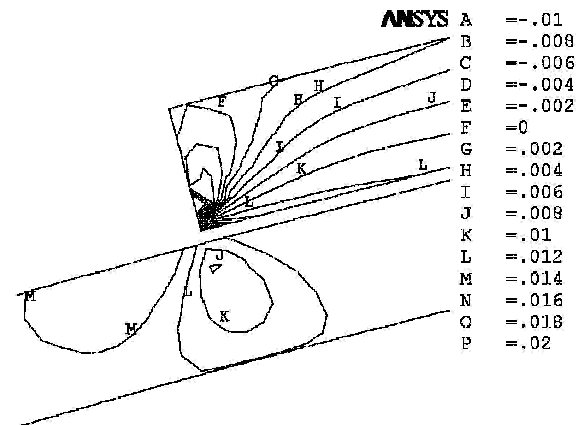


**Figure 16c:** Circumferential strain in the adhesive near the outer end of the FRP (location A)

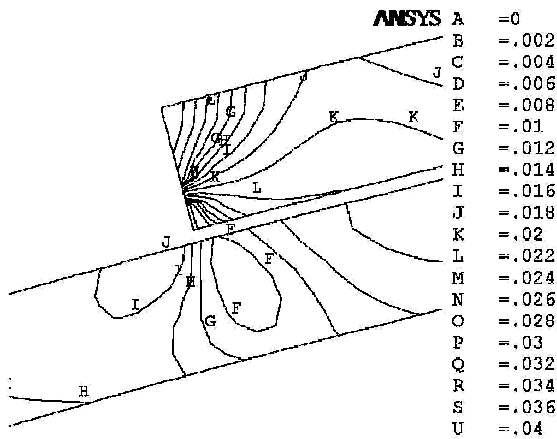


**Figure 16d:** von Mises strain in the adhesive near the outer end of the FRP (location A)

## 7 Conclusions

This paper has presented a finite element analysis which gives a useful explanation for the failure of FRP strengthening for concrete or concrete filled steel tubular columns at a significantly lower failure strain than the ultimate tensile strain of FRP determined from flat coupon test. Current design and analysis methods assume that the FRP strengthening can be modelled as a simple ring that reacts a uniform internal pressure from the confined concrete. This analysis has shown that the geometric discontinuities due to the ends of the strengthening result in substantially increased local strains in both the FRP and the bonding adhesive.

The strains are particularly high in the vicinity of the outer end of the FRP, and the model predicts that these can lead to failure in two ways:

- Tensile rupture of the inner layer of FRP, in which the peak strain is about 40% higher than the “design” strain for the example problem in this paper.
- Peeling strains in the bonding adhesive within the overlapping zone. The von Mises adhesive strain is 190% higher than the uniform circumferential strain for the geometry considered.

This work is a preliminary investigation. Further work is required to examine the effects of geometry and scale, the interaction of the confined concrete with the strengthening, and to compare the analysis with experimental results.

## References

[1] Teng, J.G., Chen, J.F., Smith, S.T. and Lam, L., 2002. *FRP Strengthened RC Structures*, John Wiley and Sons, Chichester, UK.

[2] Teng, J.G., Chen, J.F., Smith, S.T. and Lam, L., 2003. Behaviour and strength of FRP-strengthened RC structures: a state-of-the-art review, *Proceedings of the Institution of Civil Engineers –*

*Structures and Buildings*, Vol.156, No. SB1, pp.51-62.

[3] Lam, L. and Teng, J.G., 2002. Strength models for fiber-reinforced plastic-confined concrete. *Journal of Structural Engineering-ASCE*, Vol.128, No.5, pp.612-623.

[4] Teng, J. G. and Lam, L., 2004, “Behaviour and modelling of fiber reinforced polymer-confined concrete”, *Journal of Structural Engineering*, Vol. 130, No. 11, pp.1713-1723.

[5] Li, G.Q, Maricherla, D., Singh, K., Pang, S.S. and John M., 2005. “Effect of fiber orientation on the structural behavior of FRP wrapped concrete cylinders”, *Composite Structures*, Vol.74, pp.475–483.

[6] Concrete Society, 2004. *Design guidance for strengthening concrete structures using fibre composite materials*. Technical Report 55 (2<sup>nd</sup> ed), Concrete Society, Crowthorne.

[7] American Concrete Institute, 2002. *Guide for the design and construction of externally bonded FRP systems for strengthening concrete structures*. ACI 440.2R-02, American Concrete Institute, Detroit.

[8] Lam, L. and Teng, J.G., 2003. Design-oriented stress-strain model for FRP confined concrete, *Construction and Building Materials*, Vol.17, No.6&7, pp.471-489.

[9] Shahawy, M., Mirmiran, A. and Beitelman, T., 2000. Tests and modelling of carbon-wrapped concrete columns, *Composites: Part B - Engineering*, Vol.31, No.6&7: pp.471-480

[10] Lam, L. and Teng, J.G., 2004. Ultimate condition of FRP-confined concrete, *Journal of Composites for Construction*, Vol.8, No.6, pp.539-548

[11] Harries, H.A. and Carey, A., 2003. Shape and ‘gap’ effects on the behaviour of variably confined concrete, *Cement and Concrete Research*, Vol.33 No.6, pp.881-890.

[12] Vinson, J.R. and Sierakowski, R.L., 1986. *The Behavior of Structures Composed of Composite Materials*, Martinus Nijhoff, Dordrecht, Boston and London.

[13] Gdoutos, E.E. and Marioli-riga, Z.P., Eds., 2003. *Recent Advances in Composite Materials*, Kluwer academic, Dordrecht, Boston and London.